04

Effects of supersonic flow on pulsed surface sliding discharge characteristics

© A.S. Sazonov, I.V. Mursenkova

Department of Physics, Moscow State University,
Moscow, Russia
e-mail: as.sazonov@physics.msu.ru

Received August 1, 2025
Revised October 1, 2025
Accepted October 1, 2025

The results of an experimental study of current and emission characteristics of a pulsed surface sliding discharge in supersonic air flows with Mach numbers ranging from 1.20 to 1.70 and gas densities from 0.01 to 0.32 kg/m^3 are presented. A 500 ns discharge was initiated in a single-pulse mode at a voltage of 25 kV; the peak discharge current reached 1 kA. The length of the discharge region along the flow direction was approximately 100 mm. Measurements of discharge current and emission characteristics were performed in both uniform flows and in flows with an inclined shock wave. It is shown that the non-uniform density distribution in the boundary layer of a supersonic airflow results in distinctive features in the discharge current behavior and spatial radiation distribution compared to stationary air.

Keywords: nanosecond surface sliding discharge, discharge current, glow distribution, supersonic flow.

DOI: 10.61011/TP.2026.03.63157.191-25

Introduction

Various types of surface discharges are gaining increasingly greater importance due to their potential in supersonic flow control in aerodynamics. The opportunity to vary flow characteristics, in particular, of the boundary layer via plasma exposure opens the ways for increasing the efficiency of flow control. Submicrosecond surface sliding discharge is one of the promising types of discharge for aerodynamics applications.

Since the late 20th century until the present day, the surface sliding discharge has been effectively used as a source of quasi-uniform plasma in powerful gas-discharge CO_2-lasers, excimer lasers, ultraviolet light sources [1–6]. Discharge plasma radiation spectrum has its maximum in the ultraviolet range and can reach the soft X-ray region [2,7]. In air, the spectrum is mainly defined by the bands of the second positive nitrogen system [8–10].

In classical surface sliding discharge configuration, a high voltage pulse is applied to the initiating electrode placed on a dielectric plate. The grounded electrode is placed on the edge of the dielectric and extends along the back side of the plate. In such configuration, when high voltage is applied, high-strength electric field is formed in gas with prevailing normal component to the dielectric surface [2,3,7]. This field induces high-power gas ionization and plasma in the near-surface layer. Practical applications of the surface sliding discharge are primarily driven by the spatial uniformity of the generated plasma. Pulse leading edge steepness of high voltage on the initiating electrode is an important variable.

In the monopulse mode, uniformity of the distributed surface sliding discharge is attributed to a set of interconnected variables such as charge voltage, voltage pulse edge steepness, dielectric thickness and permittivity [3], and to the presence of distributed dielectric capacity, defining the uniform propagation of surface sliding discharge at high reduced electric field E/N (E is the electric field strength, N is the gas molecule concentration). Increased value of the reduced electric field in the surface sliding discharge is caused by high normal field component to the dielectric at the initial stage of ionization wave propagation over the dielectric, leading to active formation of electron avalanches [3,11]. Optical studies of a plasma layer generated by the surface sliding discharge at atmospheric pressure [2] made it possible to measure the reduced electric field by processing radiation spectra in a range of 300–900 nm. The reduced electric field was (500 ± 100) Td in different experiment conditions, indicating that the electric field in discharge is stable. Radiation is induced by processes associated with direct collisions of electrons with gas molecules. In regions with high electric field strength, intense molecule ionization and excitation take place, leading to higher emittance of these regions.

The first studies of surface sliding sparks on thin film dielectric surfaces [1] have shown that breakdown of gaps with a length up to 140 cm occurs during several half-periods when high voltage is applied. Minimum breakdown voltage depends on the discharge length, dielectric thickness and permittivity. When breakdown voltage is applied, the surface sliding discharge develops in the form of a set of channels with different intensity, the number of which

increases as the overvoltage grows. Discharge propagation is self-consistent: intensity of ionization processes is defined by channel conductivity, which depends on ionization processes, therefore the field strength is the governing parameter. When a voltage pulse is applied, bias current occurs on the dielectric surface and is defined by the charge voltage U, voltage pulse leading edge steepness dU/dt and variable capacity C between the surface discharge and initiating electrode [2]. For uniform discharge current spreading with a significant electrode length, an additional peaking capacity is included in the circuit. Current in the surface sliding discharge, repetitively-pulsed mode, and monopulse mode flows in one or two stages [3]. The first stage is characterized by the distributed dielectric capacity charge current. At this stage, the ionization wave moves from the high-voltage electrode to the grounded electrode, and the prebreakdown current plays a role of intense and uniform ionization. The second stage is a breakdown of a pre-ionized gas layer at the dielectric surface. It is characterized by the maximum power, starts from the time when the ionization wave arrives at the grounded electrode, and the energy is embedded into the plasma layer. The intense second current peak occurs in this case, and the storage capacity is discharged through a set of high current channels, reaching 6 to 10 channels per centimeter of the discharge gap length. With positive polarity of the voltage pulse, the discharge is more uniform and provides a higher energy deposition in gas [3]. Studies of the surface sliding discharge on the dielectric surface have shown that the discharge is localized near the dielectric surface, has a thickness less than 1 mm [13] and can be obtained in nitrogen and air at repetition frequencies up to 10 kHz in a wide pressure range [14]. Numerical simulation of the surface sliding discharge in vacuum [15] made it possible to determine the best conditions for gas ionization , determine electron temperature, spatial profiles of density and charge distributions of ions. The proposed computational model describing discharge propagation near the dielectric surface has shown good agreement with experimental data.

Gas flow control using gas discharge plasma has become a new area of research in aerodynamics [8,10,16–18]. Using discharges as plasma actuators generally requires a large space for surface plasma arrangement to increase the flow interaction region. In the experiments, flow was exposed to different types of discharges, and the action of surface dielectric barrier discharge is still the best known [16,19–21]. Experiments performed in shock tube have shown that it could be effectively used to control disturbances in the boundary layer, separation and vortices on aircraft wings, and aeroacoustic properties [16,18,21]. Numerical simulation has shown that a nanosecond plasma actuator with a dielectric barrier can affect the region of interaction between a shock wave and boundary layer [16]. This emphasizes the importance of further experimental studies of pulsed discharges in high-velocity flows for optimization of discharge parameters. Unlike the low-current dielectric barrier discharge, the surface sliding discharge refers to high-current discharges with kiloampere currents [1–4]. Creeping discharge in a three-electrode configuration was studied in still air [17,18], and streamer propagation intensity and rate were influenced by DC voltage applied to the third electrode. Discharge-induced shock waves were qualitatively analyzed using Schlieren imaging and pressure measurements [17]. It has been shown that a series of repeating nanosecond pulses could significantly change the discharge-generated shock wave, and the maximum flow rate and vorticity induced by the surface sliding discharge exceeded the similar parameters for dielectric barrier discharge [18]. All these factors increase the degree of discharge impact on the flow, which is especially important for aerodynamic flow control [19,20]. Comparative analysis of flows induced by surface dielectric barriers and surface sliding discharges [22] has shown that an additional electrode in the surface sliding discharge configuration also affected the space charge distribution and the characteristics of effective forces while retaining the same electric parameters.

In supersonic air flows, distributed surface sliding discharge in classical configuration was initiated in different conditions [8–10,23–25]. Differences in discharge current, spatial distribution of radiation intensity in supersonic flows with different rates and densities were reported [8,10,23,24]. Shock wave dynamics caused by the fast energy deposition in a limited gas volume has been studied comprehensively in still air and uniform high-velocity flows [8,23]. Description of discharge modes in nonuniform supersonic flows, determination of plasma properties, and study of flow effect on discharge characteristics are still important at this point.

The purpose of this work was to perform experimental study of pulsed current characteristics and nanosecond surface sliding discharge emission by initiating in supersonic air flows with the Mach numbers ranging from 1.20 to 1.70, including nonuniform density distribution with an oblique shock wave in the channel. Fourier expansion of time dependences into harmonics and their comparison in still air and in air flow were the main pulsation analysis methods.

1. Description of experiments

Experimental system consists of a shock tube with a discharge chamber (Figure 1, *a*, [8–10]). The low pressure chamber contained test gas — air at initial pressure up to 190 Torr (0.32 kg/m^3); the high pressure chamber contained helium at a pressure up to 10 atm. Self-rupture of a diaphragm between sections induced shock waves in the shock tube, after which supersonic flows with the Mach numbers ranging from 1.20 to 1.70 propagated. Shock waves and flows moved along a straight rectangular channel and reached the discharge chamber (cross-section dimensions — 24×48 mm). Air density in the experiments varied in the range of 0.01–0.32 kg/m^3.

Synchronization of the discharge system with the shock wave passage time was performed using piezoelectric transducers placed in the shock tube bore. Discharge glow was detected through quartz glasses (plane-parallel walls of the discharge chamber) by photo cameras and an electron-optical camera.

In the experiments, discharge was generated in still air, uniform supersonic flows and flows with oblique shock waves. Oblique shock waves were formed when flowing past an obstacle placed on the bottom wall of the discharge chamber (Figure 1, *b*, [9,10]). The surface sliding discharge with a duration of $\sim$ 500 ns and length of 100 mm along the main flow direction was initiated on the top wall.

Discharge was initiated using an electric circuit with a controlled discharger (Figure 2) [8,10]. The electrode system was made of a 1 mm glass fiber plastic plate, foil-coated on both sides; copper foil areas were partially removed by etching. The circuit included a storage capacitor with capacity $C_0 = 2300$ pF and peaking capacitor C_1. Creeping discharge features relatively high distributed resistance of the thin plasma channel, which stabilizes discharge and ensures consistent energy application via single pulsed excitation. Polarity of the initiating electrode was positive.

When a voltage of 25 kV was applied, discharge current reached 1–2 kA. Discharge glow was detected through quartz windows in the discharge chamber by photo cameras and an electron-optical camera. Current was measured using a special low-inductance shunt [8,10]. Electron-optical chamber operated in streak mode with a total duration up to 2000 ns (spectral range 380–800 nm).

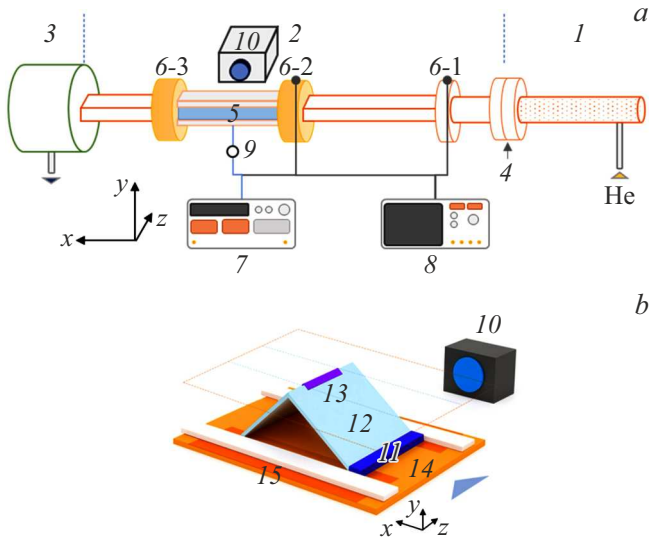

Figure 1. Experimental setup: *a* — shock tube with a discharge chamber: *1* — high pressure chamber, *2* — low pressure chamber, *3* — absorbing drum, *4*— diaphragm, *5* — discharge chamber, *6* (-1, -2, -3) — piezoelectric pressure transducers, *7* — pulse generator, *8* — oscilloscope, *9* — shunt, *10* — photo camera/electron-optical camera; *b* — flow with oblique shock wave in the discharge region: *11* — obstacle, *12* — oblique and reflected shock waves, *13* — discharge channel, *14* — glass fiber plastic, *15* — discharge electrodes.

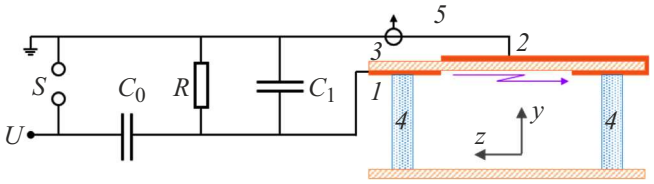

Figure 2. Circuit diagram of the surface sliding discharge: *1* — high-voltage electrode; *2* — grounded electrode; *3* — dielectric; *4* — quartz glasses; 5 — shunt; C_0 — storage capacity (2300 pF); C_1 — peaking capacity (470 pF); *R* — charge resistance (1 kΩ); *U* — voltage (25 kV); *S* — controlled discharger.

2. Experimental results and discussion

2.1. Analysis of current curves

An oscillation process with exponential current decay occurred in the discharge circuit after gap breakdown. The surface sliding discharge current in still air has a form of damped oscillations with a period of about 210–230 ns (Figure 3). The maximum current amplitude reached $\sim$ 1.5 kA, and the typical full decay time was 500–700 ns (Figure 3–5). The onset time of the current rise and, consequently, of voltage decay, was nominally taken as the time of breakdown. Fourier-series expansion was performed for waveform analysis (Figure 3–5). The obtained amplitude frequency response curves demonstrated a pronounced dependence on medium density: increase in density in still air and uniform supersonic flows led to reduction of the fundamental harmonic amplitude with a frequency of about 5 MHz (Figure 6). This harmonic is defined by the main storage capacity and inductance of circuit input elements, and by the variable resistance of the plasma layer via discharge channel propagation. At air pressures up to

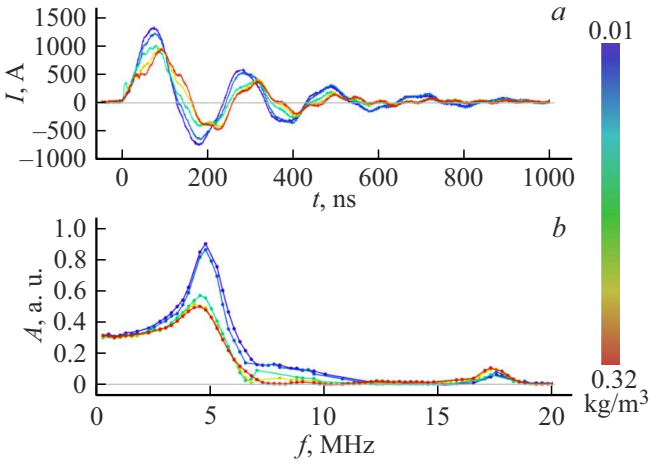

Figure 3. Waveforms of surface sliding discharge current in still air (*a*) and corresponding Fourier expansions in frequencies (*b*). Color scale is linked to air density.

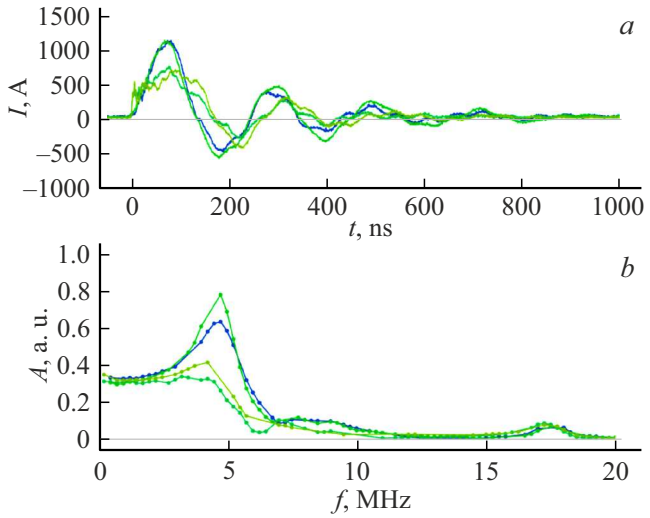

Figure 4. Waveforms of surface sliding discharge current in uniform air flows (*a*) and corresponding expansions in frequencies (*b*). Color scale is shown in Figure 3.

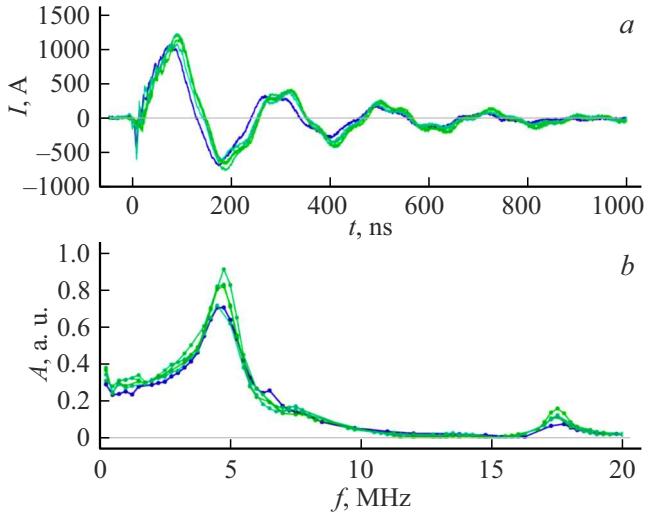

Figure 5. Waveforms of surface sliding discharge current in air flows with an oblique shock wave (*a*) and corresponding expansions in frequencies (*b*). Color scale is shown in Figure 3.

60 Torr (density up to 0.10 kg/m^3), the form of current is close to monotonic damped harmonic oscillations with a dominant frequency of ~ 5 MHz. As the air density increases, decrease in the current maximum, variation of decay behavior, occurrence of additional harmonic with a frequency of about 7.3 MHz are observed. Further increase in pressure leads not only to broadening of the fundamental harmonic maximum, but also to complication of the current oscillation frequency content.

Similar dependence of discharge current amplitude frequency response on medium density is observed in uniform supersonic air flows (Figure 4). As the density increases, the fundamental harmonic maximum becomes less sharp compared with still medium. In nonuniform supersonic flows with an oblique shock wave, current oscillations are close to harmonic ones in the given conditions. Oscillation decay time can reach 1000 ns (Figure 5). Fundamental and additional harmonic amplitudes exceed the values observed in uniform conditions and the fundamental harmonic maximum becomes more pronounced and narrow. Amplitude frequency response curves in all given modes always have a component with a frequency of about 17.5 MHz, which can be caused by resonance phenomena in the discharge circuit.

The detected differences in surface sliding discharge current oscillations in supersonic flows are certainly caused by electron multiplication in the medium in different conditions in the electric field application region. Reduced electric field strength and, accordingly, electron concentration are directly related to the discharge current flow arrangement. Only the mean electric field strength $E$with respect to the discharge gap can be analyzed experimentally in this case. In uniform medium conditions, as the density grows, E/N decreases, concentration of electrons decreases, effective plasma resistance increases, leading to greater current oscillation decay in the circuit. Note that a significant spread of the fundamental harmonic amplitude at an air density higher than 0.10 kg/m^3 is observed in uniform supersonic flows (Figure 6). This is apparently associated with turbulence propagation in the boundary layer and discharge channel geometry variation [8,23]. In conditions of nonuniform flow with an oblique shock wave, current flows via a single localized channel formed in the region of decreased gas density and, consequently, of higher reduced electric field [9,10,24,25]. Air density distribution in the supersonic flow near the oblique shock wave has a complex configuration with decreased and increased density regions [25]. Numerical gas dynamic calculations have shown that the minimum density in the area of interaction between the oblique shock wave and boundary layer is 0.4–0.7 of the incoming flow for the given range of conditions. High concentration of electrons occurs in the discharge channel, leading to a lesser decay of current oscillations with a comparatively low resistance.

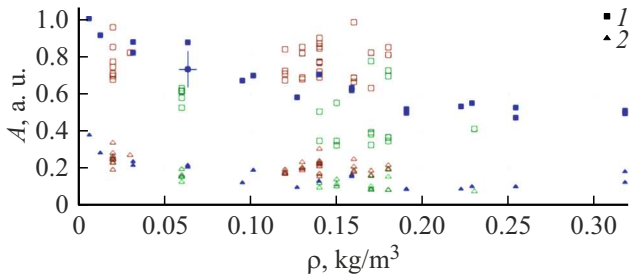

Figure 6. Fundamental current oscillation amplitudes vs. air density. Color coding: still air (blue), uniform flows (green) and flows with an oblique shock wave (red). *1* — harmonic ~ 5, *2* — ~ 7.3 MHz.

2.2. Analysis of radiative characteristics

Detection of surface sliding discharge glow by photo cameras and electron-optical camera with nanosecond time resolution has identified considerable differences in the radiation behavior depending on medium conditions and flow structure (Figure 7). Creeping surface discharge glow in still air is sufficiently uniform throughout the discharge gap length. Uniform diffuse glow in visible range is observed at low pressures. As the pressure increases, radiation evolves in the form of many relatively bright plasma channels (Figure 7, *a*).

In uniform supersonic air flows, surface sliding discharge glow was determined by the boundary flow layer state [8–10,23]. Glow distribution correlated with density fluctuation distribution because the local reduced electric field E/N defines the local concentration of electrons and, accordingly, the local plasma radiation intensity. In regions with lower density, radiation intensity is higher and, therefore, discharge channel bending can be observed in the turbulent boundary layer (Figure 7, *b*).

In nonuniform supersonic flows containing oblique shock waves, glow is concentrated in a narrow channel formed in a low gas density region (Figure 7, *c*, [9,10,24]). A strongly pronounced localized plasma channel with high afterglow intensity and duration of several microseconds is formed near the zone of interaction between the incident shock wave and boundary layer [24]. Visualization of its structure is difficult due to a wide dynamic intensity range: the brightest region is overexposed, while the adjacent regions may turn out to be underexposed. Figure 7, c, shows a photograph of the channel made with minimum opening of the photo camera aperture.

Temporal dynamics of glow was studied using the electron-optical streak camera sensitive to radiation ranging from 380 nm to 800 nm (Figure 8). The main contribution to discharge radiation is made by the second positive molecular nitrogen system, which covers the range of 280–500 nm [8,10,23]. Thus, the electron-optical camera detects the 380–500 nm range of the second positive nitrogen system. For glow streak analysis, the total glow intensity was calculated by the visible discharge width. Regions with overexposure near bright channels were avoided during processing due to data distortion. The obtained time dependences normalized to the intensity maximum are shown in Figure 9.

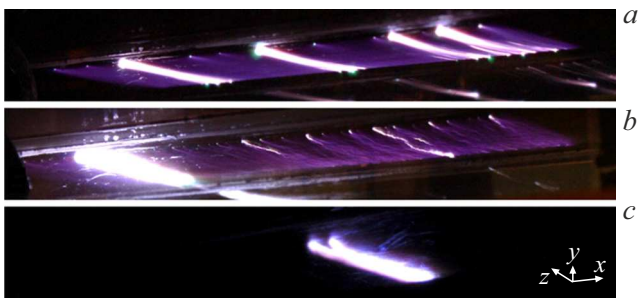

Figure 7. Photographs of surface sliding discharge: *a* — in still air; *b* — in uniform flow, $M_f = 1.39$; *c* — in flow with an oblique shock wave, $M_f = 1.32$. Density is 0.11 kg/m^3.

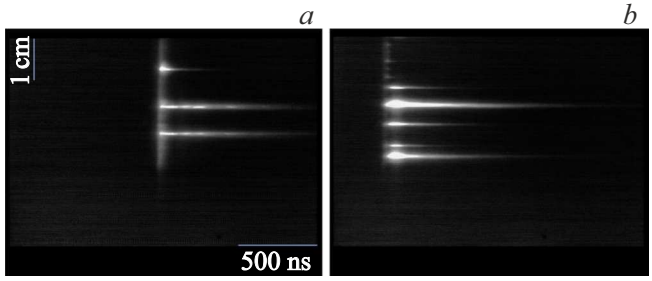

Figure 8. Discharge glow streaks in still air: *a* — at 25 Torr (density 0.04 kg/m^3), *b* — 125 Torr (0.21 kg/m^3).

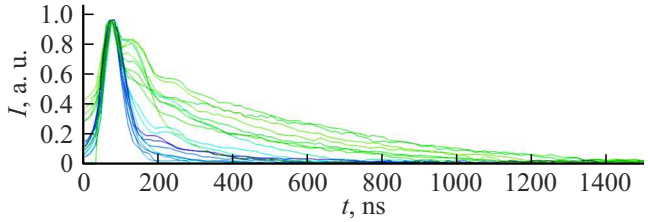

Figure 9. Time dependences of discharge radiation intensity in still air in the density range of 0.02–0.20 kg/m^3. Color scale is linked to air density (Figure 3).

Time evolution of glow is characterized by a rising phase lasting for ~ 80 ns, followed by a pulsation intensity phase and then by a long afterglow phase lasting more than 1 μs (Figure 9). The first glow maximum correlates with the circuit current maximum, while additional intensity maxima are observed during the current passage time. They are exceptionally well pronounced at a density greater than 0.10 kg/m^3. Then there is exponential intensity decay, whose behavior depends on air density. An additional maximum is detected at a density greater than 0.17 kg/m^3, that is delayed by approximately 60 ns with respect to the base peak and is not related to the current minimum. The presence of this maximum can indicate that additional current harmonics affect the discharge glow. Note that the oscillatory discharge current behavior is reflected on the glow behavior to a lesser extent. This can be attributed to the predominant energy deposition in the first oscillation half-period as well as to features of radiative processes in plasma.

Conclusion

The experimental studies of current and radiative characteristics of the pulsed surface sliding discharge in still air, uniform and nonuniform supersonic air flow conditions (Mach numbers of 1.20–1.70, density of 0.01–0.32 kg/m^3) allowed to establish key patterns of interaction between discharge and flow.

It has been established that the flow structure and density of medium have a fundamental effect on the discharge current behavior and radiation mode. The main focus has been made on the comparative Fourier analysis of current oscillations in supersonic air flows. Determination of the amplitude-frequency content have supplemented the results of previous studies of surface sliding discharge current. Decrease in the current maximum and oscillatory harmonics is observed in uniform medium conditions as the density of medium increases. In nonuniform flows formed with an oblique shock wave, enhancement of oscillatory current components and increase in decay time are observed due to a local increase in the reduced electric field in the low density region.

Radiation analysis has shown that the discharge morphology and local intensity are sensitive to the structure of the near-wall supersonic flow. In uniform conditions, spatial distribution of glow correlates with turbulent structures of the boundary layer, and, in the presence of an oblique shock wave, concentration of glow is displayed in the form of a narrow channel formed in the zone of the highest reduced electric field.

Comparison of current and radiative characteristics of the nanosecond surface sliding discharge in different initiation modes (in still air, uniform and nonuniform supersonic flows) in a sufficiently wide range of air densities and Mach numbers of the flow was performed and the main patterns were identified. The obtained results indicate high sensitivity of surface sliding discharge characteristics to gas dynamic parameters of the near-wall gas layer. This can define the specific aspects of using different types of surface discharges in active supersonic flow control applications.

Acknowledgments

This study was performed under the state order of the M. V. Lomonosov Moscow State University.

Conflict of interest

The authors declare no conflict of interest.

References

[1] S.I. Andreev, E.A. Zobov, A.N. Sidorov. J. Appl. Mech. Tech. Phys., **19** (3), 309 (1978). DOI: 10.1007/BF00850811
[2] V.Yu. Baranov, V.M. Borisov, A.M. Davidovskiĭ, O.B. Khristoforov. Sov. J. Quantum Electron., **11** (1), 42 (1981). DOI: 10.1070/QE1981v011n01ABEH005338
[3] V.M. Borisov, P.I. Vysikaylo, Yu.B. Kiryukhin, O.B. Khristoforov. Sov. J. Quant. Electron., **13** (10), 1408 (1983). DOI: 10.1070/QE1983v013n10ABEH004934
[4] G.N. Tsikrikas, A.A. Serafetinides. J. Phys. D: Appl. Phys., **29** (11), 2806 (1996). DOI: 10.1088/0022-3727/29/11/012
[5] A.B. Treshchalov, A.A. Lisovskiĭ. J. Opt. Technol., **79** (8), 456 (2012). DOI: 10.1364/JOT.79.000456
[6] P.P. Brynzalov, B.O. Zikrin, N.V. Karlov, I.O. Kovalev, A.V. Korablev, G.P. Kuz'min. Sov. J. Quant. Electron., **18** (10), 1232 (1988).
[7] R.E. Beverly III. J. Appl. Phys., **60** (1), 104 (1986).
[8] I.V. Mursenkova, I.A. Znamenskaya, A.E. Lutsky. J. Phys. D: Appl. Phys., **51** (5), 105201 (2018). DOI: 10.1088/1361-6463/aaa838
[9] I. Mursenkova, A. Sazonov, Yu. Liao, I. Ivanov. Scientific Visualization, **11** (3), 76 (2019). DOI: 10.26583/sv.11.3.07
[10] I. Mursenkova, I. Ivanov, P. Ulanov, Yu. Liao, A. Sazonov. J. Phys.: Conf. Ser., 1698, 012001 (2020). DOI: 10.1088/1742-6596/1698/1/012001
[11] L.N. Gall, A.G. Kuzmin. Zhurnal analiticheskoy khimii, **50** (5), 505 (1995) (in Russian).
[12] V. Lago, D. Grondona, H. Kelly, R. Sosa, A. Marquez, G. Artana. IEEE Transactions on Dielectrics and Electrical Insulation, **16** (2), 292 (2009). DOI: 10.1109/TDEI.2009.4815155
[13] V.M. Borisov, A.M. Davidovskiĭ, S.G. Mamonov, O.B. Khristoforov. Sov. J. Quant. Electron., **13** (5), 681 (1983). DOI: 10.1070/QE1983v013n05ABEH004266
[14] V.M. Borisov, F.I. Vysikailo, Yu.B. Kiryukhin, O.B. Khristoforov. *XV Mezhdunar. konf. po yavleniyam v ionizirovannykh gasakh* (Minsk, 1981), ch. II, s. 1111 (in Russian).
[15] I.V. Kurnin. Nauchnoe priborostroenie, **4** (55), 2006 (2019). (in Russian)
[16] A. Nazarian, M. Bazazzadeh, R. Khoshkhoo. Intern. J. Aerospace Eng., ID 2047162 (2021). DOI: 10.1155/2021/2047162
[17] K.D. Bayoda, N. Benard, E. Moreau. J. Appl. Phys., 118, 063301 (2015). DOI: 10.1063/1.4927844
[18] H.M. Song, M. Jia, H. Liang, Y. Wu. *Experimental investigation of the plasma aerodynamic actuation generated by nanosecond-pulse sliding discharge. Proc. 3rd Int. Conf. on Measuring Technology and Mechatronics Automation* (*ICMTMA-2011*) (Shanghai, IEEE, 2011), p. 116–119. DOI: 10.1109/ICMTMA.2011.316
[19] R. Sosa, E. Arnaud, E. Memin, G. Artana. IEEE Transactions on Dielectrics and Electrical Insulation, **16** (2), 305 (2009). DOI: 10.1109/TDEI.2009.4815157
[20] N. Benard, E. Moreau. Experiments in Fluids, **55**, Art. 1846 (2014). DOI: 10.1007/s00348-014-1846-x
[21] A.Yu. Starikovskiy, N.L. Aleksandrov. Plasma Phys. Rep., **47** (2), 148 (2021).
[22] P.A. Polivanov, O.I. Vishnyakov, A.A. Sidorenko, A.A. Maslov. J. Appl. Mech. Tech. Phys., **54** (3), 359 (2013). DOI: 10.1134/S0021894413030036
[23] I.A. Znamenskaya, D.F. Latfullin, I.V. Mursenkova. Techn. Phys. Lett., **34** (8), 668 (2008).
[24] I.V. Mursenkova, A.F. Ziganshin. Techn. Phys. Lett., **50** (10), 11 (2024). DOI: 10.61011/PJTF.2024.10.57702.19791
[25] I.V. Mursenkova, I.E. Ivanov, Y. Liao, A.F. Ziganshin. Plasma Phys. Reports, **49** (6), 795 (2023). DOI: 10.31857/S0367292123600164

Translated by E.Ilyinskaya